

## PAPER

# Local–Global Multimodal Contrastive Learning For Molecular Property Prediction

Xiayu Liu ,<sup>1</sup> Zhengyi Lu ,<sup>2</sup> Yunhong Liao ,<sup>3</sup> Chao Fan ,<sup>4</sup> and Hou-biao Li ,<sup>1,\*</sup>

<sup>1</sup>School of Mathematical Sciences, University of Electronic Science and Technology of China, No.2006, Xiyuan Avenue, West Hi-tech Zone, 611731, Chengdu, China, <sup>2</sup>Department of Computer Science and Engineer, Oakland University, 201 Meadow Brook RD, Rochester Hills, 48309, MI, USA, <sup>3</sup>Department of Electrical and Computer Engineering, Oakland University, 201 Meadow Brook Rd, Rochester Hills, 48309, MI, USA and <sup>4</sup>College of Management Science, Chengdu University of Technology, No.1, East Third Road, Erxianqiao, Chenghua District, 610051, Chengdu, China

\*Corresponding author: Hou-biao Li, lihoubiao0189@163.com

FOR PUBLISHER ONLY Received on Date Month Year; revised on Date Month Year; accepted on Date Month Year

## Abstract

Accurate molecular property prediction requires integrating complementary information from molecular structure and chemical semantics. In this work, we propose LGM-CL, a local-global multimodal contrastive learning framework that jointly models molecular graphs and textual representations derived from SMILES and chemistry-aware augmented texts. Local functional group information and global molecular topology are captured using AttentiveFP and Graph Transformer encoders, respectively, and aligned through self-supervised contrastive learning. In addition, chemically enriched textual descriptions are contrasted with original SMILES to incorporate physicochemical semantics in a task-agnostic manner. During fine-tuning, molecular fingerprints are further integrated via Dual Cross-attention multimodal fusion. Extensive experiments on MoleculeNet benchmarks demonstrate that LGM-CL achieves consistent and competitive performance across both classification and regression tasks, validating the effectiveness of unified local-global and multimodal representation learning.

**Key words:** molecular property prediction, contrastive learning, multimodal learning

## Introduction

Molecular property prediction plays a fundamental role in modern drug discovery and chemical research, as it enables the efficient estimation of physicochemical, biological, and toxicological properties of candidate molecules prior to costly experimental validation. Accurate prediction of molecular properties such as bioactivity, solubility, permeability, toxicity, and binding affinity can significantly accelerate the early stages of drug development, reduce experimental costs, and improve the success rate of lead compound identification.

Early computational approaches to molecular property prediction primarily relied on handcrafted molecular descriptors and fingerprints, including physicochemical descriptors and substructure-based features [1, 2, 3]. These representations were typically combined with conventional machine learning algorithms such as Support Vector Machines (SVM) [4], and Random Forests (RF) [5]. While such methods achieved encouraging performance on various tasks, their predictive capability heavily depends on manually crafted descriptors, which often fail to fully capture complex chemical interactions. Consequently, these approaches may struggle to generalize across chemically diverse prediction scenarios

With the rapid advancement of deep learning, a wide range of neural architectures have been proposed for molecular property prediction [6]. In contrast to traditional approaches, deep models can automatically learn task-specific molecular representations directly from raw molecular structures. In particular, graph neural networks (GNNs) have gained widespread adoption due to their natural compatibility with molecular graph structures, where atoms and bonds are represented as node and edges, respectively. Message passing paradigms [7, 8, 9, 10, 11] iteratively aggregate local chemical information to generate molecular embeddings. Meanwhile, transformer architectures have been introduced to molecular representation learning to better address long-range and global dependencies through self-attention mechanisms [12, 13, 14, 15]. Despite their effectiveness, existing approaches still face challenges in jointly modeling molecular information across different structural scales.

Molecular properties are intrinsically governed by chemical patterns at multiple structural scales. Local chemical environments, such as functional groups and atom-level neighborhoods, determine reactivity and local chemical behavior [16], whereas global molecular context, including long-range dependencies and overall topology, influences macroscopic properties such as stability, solubility, and

bioactivity [17]. However, existing molecular representation learning methods often emphasize either local or global structure. Localized message passing approaches excel at capturing neighborhood level interactions but may inadequately encode global dependencies, while models designed for long-range modeling may overlook subtle local chemical patterns. This imbalance motivates the explicit integration of local and global molecular information as complementary components for molecular representation learning.

Beyond graph-based representations, molecular properties are also closely related to chemical patterns encoded in molecular strings. The Simplified Molecular Input Line Entry System (SMILES) [18] provides a linearized description of molecular structure, preserving sequential patterns and implicit chemical rules. Inspired by advances in natural language processing, SMILES strings have been increasingly utilized as an alternative representation for molecular property prediction using transformer-based language models [19]. However, SMILES representations primarily capture structural syntax and may offer a limited view of higher level physicochemical attributes. Recently, large language models (LLMs) have been explored to generate chemically relevant textual descriptions as auxiliary molecular representations [20, 21, 22]. While promising, the application of LLM-generated content introduces the risk of hallucination, where chemically incorrect or unsupported information may be produced [23]. Mitigating hallucination therefore requires constraining the generation process through chemistry-aware prompting strategies, enabling LLM-generated text to serve as a reliable and complementary view.

Taken together, these observations suggest that molecular property prediction is inherently a multiview problem [24, 25], where different representation modalities capture complementary aspects of molecular information. Graph-based representations emphasize molecular topology and multiscale structural interactions, while sequence- and text-based representations provide additional semantic perspectives derived from linearized structure and chemically informed knowledge. Relying on any single modality is therefore insufficient to fully characterize complex structure-property relationships.

Learning unified representation from heterogeneous molecular modalities remains challenging problem due to differences in feature distributions and inductive biases. In this context, contrastive learning provides a principled framework for multimodal representation learning by aligning multiple views of the same molecule in a shared embedding without explicit supervision [26, 27, 28]. By encouraging consistency across complementary modalities, contrastive objectives enable the learning of robust and transferable molecular representations while mitigating the limitations of individual views.

To address the above challenges, we propose LGM-CL, a unified Local–Global Multimodal Contrastive Learning framework for molecular property prediction. Starting from SMILES strings, LGM-CL constructs multiple complementary molecular views that capture local structural patterns, global topological context, and physicochemical knowledge at different levels. Structural information is modeled from molecular graphs to characterize both local functional group environments and global molecular organization, while textual information is derived from SMILES strings and chemically informed descriptions to encode physicochemical characteristics beyond pure structural syntax.

LGM-CL adopts a self-supervised multiview contrastive learning strategy to effectively align heterogeneous molecular representations without relying on task-specific supervision. By contrasting different structural and textual views of the same molecule, the framework learns consistent and transferable molecular embeddings that integrate local and global structure cues with chemically meaningful semantic information. For downstream molecular property prediction, the learned representations are further refined by incorporating molecular fingerprints as an additional complementary modality, enabling unified fusion of structural, semantic, and fingerprint-based information.

The main contributions of this work are summarized as follows:

- We propose a chemistry-aware prompting template for SMILES augmentation, which reduces hallucination in LLM-generated text and enables self-supervised contrastive learning between original SMILES and chemically enriched textual descriptions.
- We introduce a local–global contrastive graph representation learning scheme, where molecular graphs are encoded by separate local and global encoders to jointly capture functional group information and global topological context.
- We develop a unified multi-modal framework (LGM-CL) that integrates textual, graph-based, and molecular fingerprint representations to learn transferable molecular embeddings for property prediction.
- Extensive experiments on multiple benchmark datasets demonstrate the effectiveness of LGM-CL, with ablation studies and visualization analyses validating the contribution of each component.

## Materials and methods

### Overview of Model

Our framework aims to learn a chemically meaningful and transferable molecular representation by unifying local function group patterns, global topological context and physicochemical semantics derived from SMILES and LLM-enhanced textual descriptions, through self-supervised multi-view contrastive learning and cross-modal attention-based fusion. Starting from SMILES strings, we construct multiple complementary molecular views that capture structural and semantic information at different levels. Specifically, we build a graph-based view that explicitly models both local neighborhood structures and global topological dependencies by employing distinct graph encoders, and a text-based view constructed from original SMILES strings together with chemistry-aware textual augmentations that emphasize physicochemical semantics.

We first apply a set of self-supervised multi-view contrastive learning objectives over these representations, including view-specific objectives for the graph and text modalities, as well as cross-view objectives that encourage consistency between complementary representations of the same molecule. For the graph modality, different structural views derived from the same molecular graph are jointly contrasted to emphasize both local function group information and global molecular context. For the text modality, chemically enriched descriptions generated from SMILES are contrasted with their original string-based representations, enabling the textual encoder to capture domain-specific physicochemical semantics

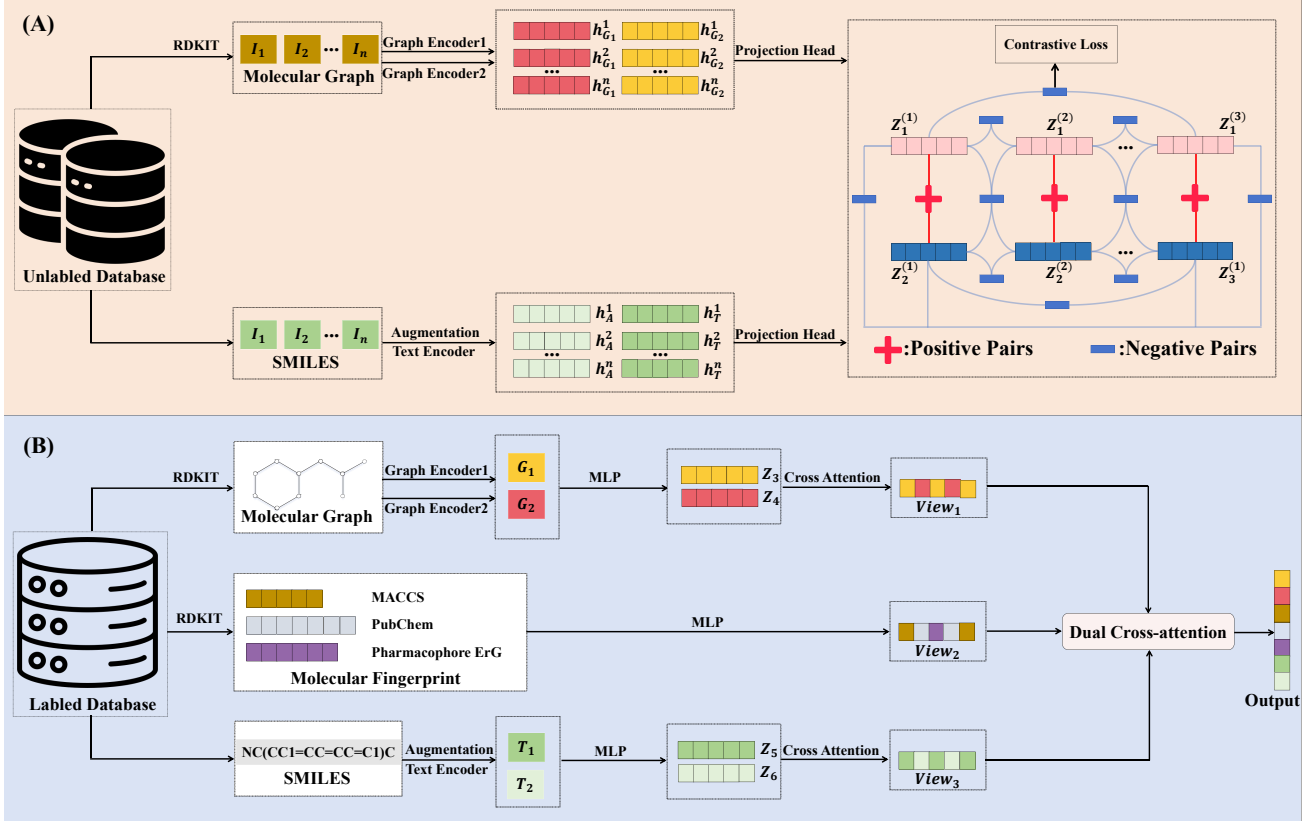


Fig. 1. Overview of Model. (A) Pipeline of the model in the pre-training stage. (B) Pipeline of the model when applied to downstream tasks.

beyond pure syntactic structure. Through this multi-view contrastive pretraining, the model learns transferable molecular representations that integrate local and global structural information with chemically meaningful semantic knowledge.

Following the multi-view contrastive pretraining stage, the model is further adapted to downstream tasks in a fine-tuning stage by incorporating molecular fingerprint information as an additional complementary modality. In this stage, pretrained graph- and text-based representations are first consolidated within each modality to form unified graph and text embeddings, and are then jointly aligned with fingerprint-based features through a Dual Cross-attention module to obtain a single molecular representation for prediction. This hierarchical integration strategy enables effective fusion of structural, semantic, and fingerprint-derived information while preserving their complementary roles. An overview of the model is provided in Figure 1.

### Graph Modality Contrastive Learning

Inspired by the dual-view contrastive learning paradigm proposed in DGCL [30], we design a graph modality contrastive learning strategy that explicitly captures molecular information at different structural scales. To this end, we employ two structurally complementary graph encoders to generate distinct yet semantically consistent representations of the same molecular graph. The two encoders are designed to focus on complementary structural scales of the molecular graph, corresponding to a global view and a local view, respectively, as described below. An overview of the two encoders is illustrated in Figure 2(A) and Figure 2(B), respectively.

### Global Graph Encoder via Graph Transformer

Accurate molecular property prediction often requires modeling global structural dependencies, as small local modifications may lead to substantial changes in molecular activity, a phenomenon commonly referred to as activity cliffs. Capturing such long-range interactions and holistic molecular context is therefore critical for robust prediction. Motivated by this observation and following prior work [33, 34, 35, 36], we adopt a graph transformer as a global graph encoder to account for long-range dependencies and global molecular structure. Given an arbitrary SMILES sequence  $S$ , we first convert it into a molecular graph  $G = (V, E)$  using RDKIT, where  $V$  and  $E$  denote the sets of atoms and bonds, respectively. Each atom  $v_i \in V$  and bond  $e_k \in E$  is initialized with a set of chemical descriptors according to a predefined encoding scheme, as summarized in Table 1. This process yields the initial atom features  $\{a_i\}_{i=1}^n$  and bond features  $\{b_k\}_{k=1}^m$ , where  $n$  and  $m$  denote the numbers of atoms and bonds in the molecule. The atom and bond features are then jointly embedded through an embedding layer, producing a node feature matrix  $M \in R^{n \times d}$ , where each row corresponds to a contextualized atom representation. Based on  $M$ , linear projections are applied to obtain the query, key, and value matrices  $Q$ ,  $K$ , and  $V$ , which are subsequently used to compute attention scores according to the graph transformer formulation. By integrating node feature interactions with adjacency-aware attention, the resulting representations enable effective propagation of information across the entire molecular graph, facilitating the modeling of long-range dependencies and global molecular structure. Specifically, the attention output for

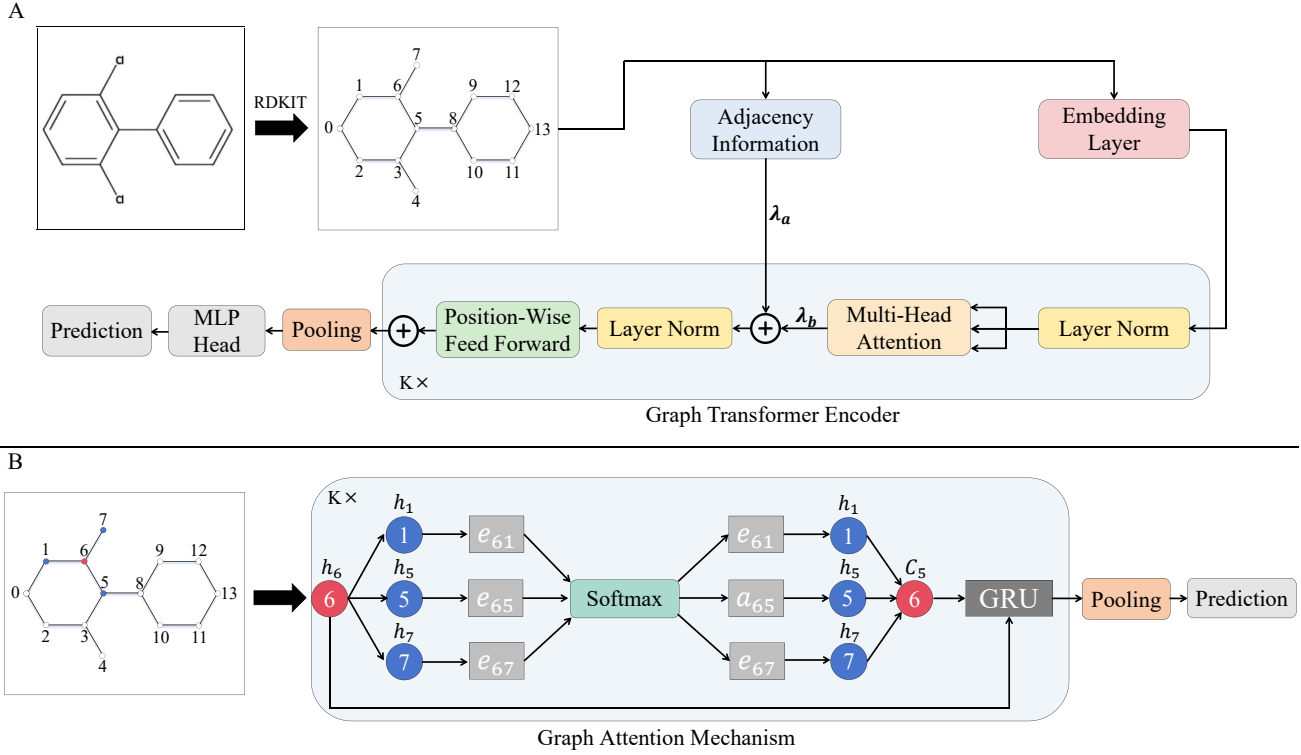


**Fig. 2.** Overview of global and local graph encoders. (A) The Graph Transformer encoder, which model global structural dependencies of molecular graphs through multi-head self-attention with adjacency-aware bias. (B) The Attentive FP encoder, which captures local chemical environments via attention-guided message passing followed by a GRU-based update and pooling operation.

each node is computed as

$$A_{score} = (\lambda_a \cdot \text{softmax}(\frac{QK^T}{\sqrt{d_k}}))V \quad (1)$$

Specifically, Eq.1 enables each node to aggregate information from all other nodes in the molecular graph through attention-weighted interactions. The scaled dot-product attention computes pairwise relevance scores between atoms, allowing the model to capture long-range structural dependencies beyond local neighborhoods. By integrating information across the entire graph, the Graph Transformer encoders global molecular context, which is essential for modeling activity cliffs where small local changes can induce substantial global effects.

#### Local Graph Encoder via Attentive FP

while global structural context plays an important role in molecular property prediction, many molecular properties are strongly influenced by local chemical environments, such as functional groups and other chemically meaningful molecular motifs. These local structures often determine key physicochemical characteristics and reactivity patterns, making their accurate modeling essential for reliable prediction. To capture such localized information, we employ Attentive FP [29] as the local graph encoder.

Attentive FP updates atom representations through an attention-guided message passing mechanism [7] that focuses on short-range chemical interactions. In our framework, we intentionally adopt a shallow Attentive FP architecture with

a small number of message passing layers, encouraging the encoder to emphasize local atomic neighborhoods and function-group-level patterns, rather than propagating information over long graph distances that are already modeled by the global graph encoder.

Following the initial feature embedding described in the previous section, each atom is associated with a contextualized node representation, forming a node feature matrix

$$M = [h_1^{(0)}, h_2^{(0)}, \dots, h_n^{(0)}]^T \in R^{n \times d} \quad (2)$$

where  $h_v^{(0)}$  denotes the initial representation of atom  $v$ . At message passing layer  $l$ , an attention score is first computed for each pair of neighboring atoms  $(v, u)$ . Specifically, the unnormalized attention coefficient is defined as

$$e_{vu}^{(l-1)} = \text{LeakyReLU}(W_{vu}^{(l-1)}[h_v^{(l-1)}, h_u^{(l-1)}]) \quad (3)$$

which measures the importance of neighbor atom  $u$  to atom  $v$  based on their representations at the previous layer. The attention coefficients are then normalized over the neighborhood  $N(v)$  using a softmax function:

$$a_{vu}^{(l-1)} = \text{softmax}(e_{vu}^{(l-1)}) = \frac{\exp(e_{vu}^{(l-1)})}{\sum_{i \in N(v)} \exp(e_{vi}^{(l-1)})} \quad (4)$$

ensuring that the contributions from all neighboring atoms sum to one. Using these attention weights, a context vector for atom

**Table 1.** Initial Atomic and Bond Features.

Atom Features	Size	Description
Atom Symbol	16	[C, N, O, F, Si, Cl, As, Se, Br, Te, I, At, others] (one-hot)
Degree	6	Number of atoms connected to the atom (one-hot)
Formal Charge	1	Electrical charge (integer)
Radical Electrons	1	Number of radical electrons (integer)
Hybridization	6	[sp, sp <sup>2</sup> , sp <sup>3</sup> , sp <sup>3</sup> d, sp <sup>3</sup> d <sup>2</sup> , other] (one-hot)
Aromaticity	1	Whether the atom is part of an aromatic system (one-hot)
Hydrogens	5	Number of hydrogens connected to the atom (one-hot)
Chirality Type	4	The chirality type of the atom (one-hot)
Ring	1	Whether the atom is in a ring (one-hot)
Ring Type	4	[3, 4, 5, 6] (one-hot)
Atomic Mass	1	Mass of the atom (integer)
Implicit Valence	7	[0, 1, 2, 3, 4, 5, 6, 7] (one-hot)
Hydrogen Acceptor	1	Whether the atom acts as a hydrogen acceptor (one-hot)
Hydrogen Donor	1	Whether the atom acts as a hydrogen donor (one-hot)
Acidic	1	Whether the atom is part of an acidic group (one-hot)
Basic	1	Whether the atom is part of a basic group (one-hot)
Bond Features	Size	Description
Bond Type	5	[exists, single, double, triple, aromatic] (one-hot)
Conjugation	1	Whether the bond is conjugated (one-hot)
Wedge Bond	2	[endupright, enddownright](one-hot)
Ring	1	Whether the bond is in a ring (one-hot)
Stereo	6	[0, 1, 2, 3, 4, 5] (one-hot)

$v$  is computed as a weighted aggregation of its neighbors:

$$c_v^{(l-1)} = \text{ELU}\left(\sum_{u \in N(v)} a_{vu}^{(l-1)} \cdot W_v^{(l-1)} h_u^{(l-1)}\right) \quad (5)$$

where the attention mechanism allows the model to selectively emphasize chemically relevant neighboring atoms and local substructures. Finally, the atom representation is updated via a gated recurrent unit (GRU) [37]:

$$h_v^{(l)} = \text{GRU}(c_v^{(l-1)}, h_v^{(l-1)}) \quad (6)$$

which integrates the newly aggregated local context while preserving previously learned atomic information. Through a limited number of such message passing layers, Attentive FP produces refined atom representations that encode rich local chemical environments, providing an effective local graph encoder complementary to the global structural component.

#### Contrastive Alignment of Global and Local Graph Representations

To jointly align global and local structural information, we introduce a contrastive learning objective between the representations learned by the global and local graph encoders. Given a molecular graph, the two encoders process the same input structure but are designed to capture complementary information at different structural scales. Specifically, AttentiveFP is employed as a local graph encoder with a shallow message passing architecture, which restricts information propagation to a limited neighborhood range. This design encourages the model to focus on local chemical environments, such as functional groups and short-range

bonding patterns that are critical for determining local reactivity and physicochemical properties. In contrast, the Graph Transformer serves as a global graph encoder by leveraging a generic self-attention mechanism, enabling each atom to attend to all other atoms in the molecular graph. This formulation allows the model to capture long-range dependencies and holistic molecular context, which are essential for modeling global structural effects and activity cliffs. For each molecular graph, atom-level representations obtained from the two encoders are aggregated via a sum-based readout to form molecule-level and local embeddings.

Although both representations are derived from the same molecular graph, they capture complementary structural information at different levels of granularity. To encourage consistency between two views, we perform contrastive learning on the corresponding representation pairs. Specifically, we adopt the Normalized Temperature-scaled Cross entropy(NT-Xent) loss as the contrastive objective. Within a mini-batch of  $N$  molecules, the global and local representations of the same molecule form a positive pair, while representations from different molecules serve as negative samples. The contrastive objective aligns local and global structural views, resulting in consistent molecular representations. The NT-Xent loss is defined as:

$$\ell(z_i, z_j) = \exp(\text{sim}(z_i, z_j)/\tau) \quad (7)$$

$$\mathcal{L}_{CL} = -\frac{1}{N} \sum_{i=1}^N \log \frac{\ell(z_{global}^{(i)}, z_{local}^{(i)})}{\sum_{k=1}^N 1_{[k \neq i]} \ell(z_{global}^{(i)}, z_{global}^{(k)}) + \ell(z_{global}^{(i)}, z_{local}^{(k)})}$$

where  $z_{global}$  and  $z_{local}$  denote the molecule-level representations obtained from the global and local graph encoders, respectively;

$1_{[k \neq i]}$  is an indicator function excluding the self-pair.  $sim(\cdot, \cdot)$  denotes the cosine similarity function and  $\tau$  is a temperature hyperparameter.

By minimizing this contrastive objective, the global and local representations corresponding to the same molecule are pulled closer in the embedding space, while representations associated with different molecules are pushed apart. This loss enforces cross-scale alignment between global and local graph representations, enabling the model to capture consistent structural semantics across different levels of granularity. As a result, the contrastive objective serves as an effective self-supervised pretraining signal that facilitates robust and informative molecular representation learning.

## Text Modality Contrastive Learning

### LLM-Based Semantic Augmentation with Prompt Templates

In order to enrich the semantic capacity of the textual modality, we augment the raw SMILES strings with chemically meaningful natural language descriptions generated by Mistral-7B-Instruct-v0.3 [31]. Although SMILES provides an effective symbolic encoding of molecular structure, it lacks explicit information about key chemical characteristics, such as function groups, reactivity patterns, stereochemical features, and broader physicochemical profiles. These semantics attributes, which are crucial for understanding molecular behavior, are not directly accessible from the SMILES content. In response to this limitation, we prompt Mistral-7B-Instruct-v0.3 with a carefully designed template to elicit descriptive textual information that reflects the underlying chemical semantics of the molecule. To guide the language model towards producing chemically reliable and semantically structured descriptions, drawing inspiration from prior studies on prompt engineering for scientific and chemical language modeling [42, 43], we design a prompt template that incorporates several elements of prompt engineering. The template begins with a role-prompting instruction, explicitly conditioning the large language model to assume the role of an expert medicinal chemist and cheminformatics scientist. This role specification encourages the model to adopt domain-appropriate reasoning patterns, terminology, and representational biases when interpreting a molecule. In addition, the template incorporates strict content constraints motivated by the known tendency of large language models to generate incorrect or fabricated numerical values. To prevent such numerical hallucinations, the model is explicitly instructed not to invent quantitative information. Furthermore, as a measure to avoid introducing task-specific biases that could interfere with downstream property prediction, the template disallows any reference to particular prediction tasks or biological endpoints. Finally, to ensure compatibility with an unsupervised contrastive learning setting, the model is restricted to producing descriptions grounded solely in the SMILES string and the accompanying RDKIT-derived descriptors, without relying on any external or task-dependent information. These constraints serve as safeguards to ensure that the generated text remains factual and chemically interpretable. Because large language models do not always adhere perfectly to a fixed output structure, we further apply a post-processing step that normalizes the generated content into a unified format. This preprocessing ensures that every molecule is represented using a consistent template, which is essential for stable contrastive learning in the subsequent stage. Workflow for enriching SMILES strings

with chemically meaningful natural language descriptors and a simplified illustration of the prompt template is shown in Figure 4, and the complete version is provided in the supplementary material.

### Contrastive Alignment of SMILES and Textual Representation

To effectively exploit the complementary information present in the two textual views, we perform contrastive learning between the raw SMILES strings and the augmented descriptions generated by the prompt-guided language model. The SMILES representation primarily conveys the molecular topological structure information, including atom connectivity, local structural patterns, and implicit geometric constraints. In contrast, the augmented text provides higher-level chemical semantics that are not explicitly accessible from the SMILES alone, including the core scaffold, salient structural features, physicochemical tendencies, and general medicinal chemistry attributes elicited through the designed prompt template. By contrasting these two perspectives of the same molecule, the model is encouraged to associate structural cues with their corresponding semantic interpretations, thereby learning a richer and more chemically informative representation. Such alignment facilitates downstream property prediction, as the learned embedding integrates both precise structural information and abstract chemical knowledge that jointly contribute to molecular behavior.

Implementing this contrastive alignment requires an encoder capable of handing both symbolic SMILES sequences and natural language descriptions with a unified architecture. For this purpose, we utilize DeBERTa [32], whose disentangled attention design enables it to effectively capture view-specific information from each of the two views. A schematic illustration of the DeBERTa architecture is provided in Figure 3(B). DeBERTa is a transformer-based language model that improves contextual representation learning through a disentangled attention mechanism, in which content and position information are encoded separately. Given a textual input  $X_i = \{x_1, x_2, \dots, x_n\}$ , DeBERTa first maps each token into a continuous representation through an embedding layer, resulting in a content embedding matrix  $H_i \in R^{n \times d}$ , where  $n$  denotes the sequence length and  $d$  is the hidden dimension. In parallel, relative positional relationships between token pairs are encoded by a relative position embedding module, producing position representations  $P_i \in R^{2k \times d}$ , where  $k$  denotes the maximum relative distance considered in the model. Based on the content embeddings  $H_i$  and the shared relative position representations  $P_i$ , DeBERTa computes attention score using a disentangled formulation that explicitly models content-to-content, content-to-position, and position-to-content interactions, as defined below:

$$\begin{aligned}
 Q_c &= H_i W_{q,c}, \quad K_c = H_i W_{k,c}, \quad V_c = H_i W_{v,c} \\
 Q_r &= P_i W_{q,r}, \quad K_r = P_i W_{k,r} \\
 \tilde{A}_{i,j} &= \underbrace{Q_i^c K_j^{c\top}}_{\text{(a) content-to-content}} + \underbrace{Q_i^c K_{\delta(i,j)}^{r\top}}_{\text{(b) content-to-position}} + \underbrace{K_j^c Q_{\delta(j,i)}^{r\top}}_{\text{(c) position-to-content}} \\
 H_i^o &= \text{softmax}\left(\frac{\tilde{A}}{\sqrt{3d}}\right) V_c
 \end{aligned} \tag{8}$$

where  $W_{q,c}, W_{k,c}, W_{v,c}, W_{q,r}, W_{k,r} \in R^{d \times d}$  are learnable projection matrices for content and positional components, respectively. The function  $\delta_{(i,j)}$  maps the relative distance

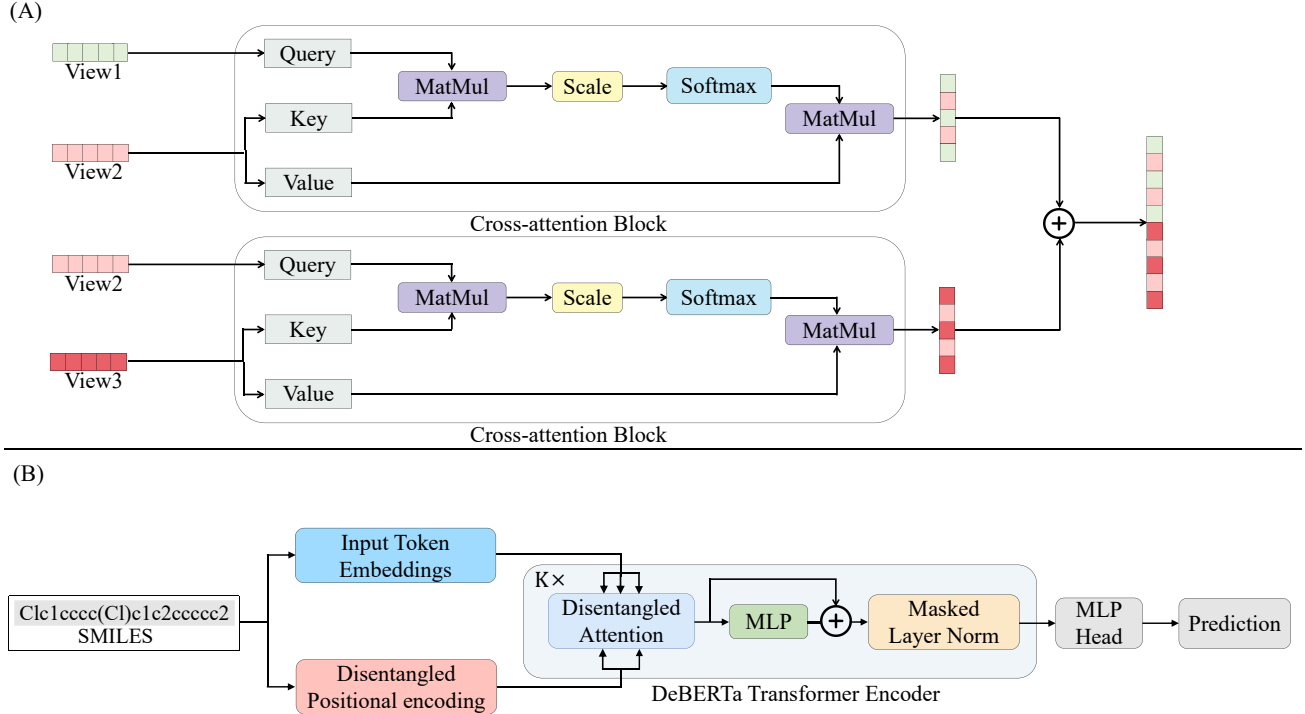


**Fig. 3.** Schematic illustration of the dual cross-attention component and text encoder in our framework. (A) The details of the dual cross-attention component. (B) DeBERTa-based encoder for SMILE and LLM-augmented textual descriptions.

between token  $i$  and token  $j$  to an index in the relative position embedding space. The attention score  $\tilde{A}_{i,j}$  is computed as the sum of content-to-content, content-to-position, and position-to-content interactions. The resulting representation  $H_o$  corresponds to the output features vectors of this attention layer and serves as the input to the subsequent layers or downstream output modules.

After encoding the SMILES string and their corresponding LLM-augmented textual descriptions with DeBERTa, we obtain two complementary textual representations for each molecule. To align these two views, we apply contrastive learning that brings representations from the same molecule closer while separating those from different molecules. Following the same NT-Xent contrastive loss defined above, the objective is formulated as:

$$\ell_{CL} = \frac{1}{N} \sum_{i=1}^N \log \frac{\ell(z_s^{(i)}, z_a^{(i)})}{\sum_{k=1}^N 1_{[k \neq i]} \ell(z_s^{(i)}, z_s^{(k)}) + \ell(z_s^{(i)}, z_a^{(k)})} \quad (9)$$

where  $z_s$  denotes the textual representation obtained by encoding the original SMILES string, and  $z_a$  denotes the representation obtained by encoding the corresponding LLM-augmented textual description. All other symbols are defined in the same manner as in Eq.7.

Through this contrastive learning objective, the model is encouraged to associate structural cues derived from SMILES with complementary semantic information provided by the augmented text, enabling the learned representations to simultaneously encode molecular topological information and chemically meaningful semantic attributes.

### Multi-Modal Fusion and Fine-Tuning

After pretraining the modality-specific encoders, we perform multimodal fusion and fine-tuning to obtain a unified molecular representation for downstream property prediction. During this stage, the pretrained graph and text encoders are reused, and their parameters are initialized from the contrastive pretraining stage.

For the graph modality, the molecular graph is processed by both the Attentive FP encoder and the Graph Transformer, producing local and global graph representations, respectively. To integrate these complementary structural features, we employ a cross-attention mechanism that aggregates the two representations into a unified graph-level embedding, enabling the model to jointly capture localized substructure motifs and functional group patterns as well as long-range topological dependencies.

For the text modality, the original SMILES string and its LLM-enhanced, chemistry-aware textual description are encoded by pretrained DeBERTa model to obtain structural and physicochemical semantic representations. These two textual representations are then fused via cross-attention to form a unified text-level embedding that combines molecular structural information with domain-specific physicochemical semantics.

In addition, multiple molecular fingerprints, including MACCS keys [38], PubChem fingerprints [39], and ErG pharmacophore fingerprints [40], are introduced as an additional complementary modality. The fingerprint vectors are projected into a latent embedding space through an

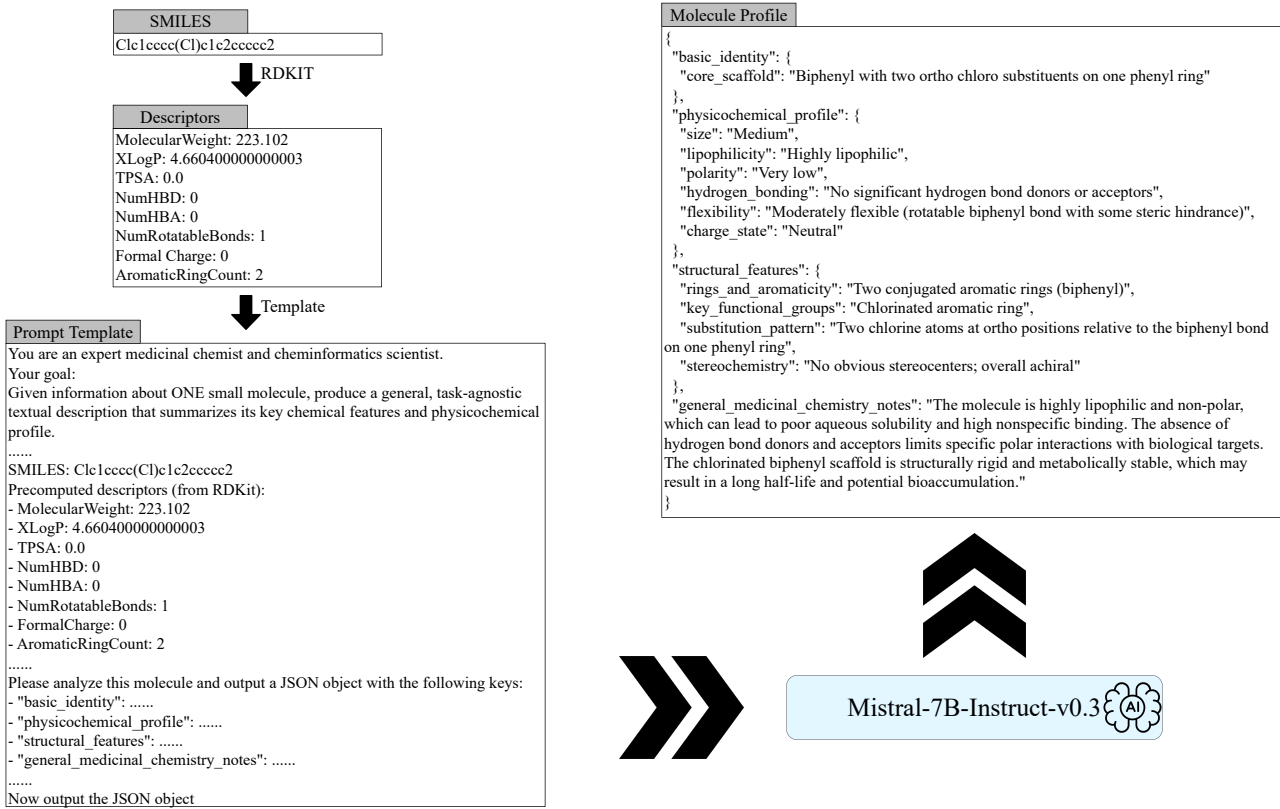


**Fig. 4.** Workflow for enriching SMILES strings with chemically meaningful natural language descriptions generated by Mistral-7B-Instruct-v0.3.

MLP, yielding a fingerprint-based molecular representation that captures substructure and pharmacophoric patterns.

After obtaining modality-specific representations for the graph, text, and fingerprint modalities, we further integrate them using a Dual Cross-attention Mechanism [44]. This module enables bidirectional interactions among heterogeneous modalities, facilitating effective information exchange and alignment across structural, semantic, and fingerprint-derived representations. The output of the Dual Cross-attention module serves as the final molecular representation.

Finally, the fused molecular representation is fed into a task-specific MLP to perform molecular property prediction. Through this hierarchical fusion and fine-tuning process, the model effectively combines local and global structural information, physicochemical semantics and fingerprint-based features, resulting in expressive and transferable molecular representations for downstream tasks.

## Experiments

### Experiments Settings

#### Datasets

For the self-supervised pretraining stage, we utilize the ZINC15 dataset [45], which contains around 330k unlabeled molecules represented by SMILES strings. This large-scale dataset provides diverse molecular structures and is widely used for pretraining molecular representation models. For downstream evaluation, we finetune the pretrained model on ten benchmark datasets from MoleculeNet [41], covering both classification and regression tasks. Specifically, the classification benchmarks

include BBBP, BACE, Clintox, Tox21, SIDER, HIV, and ToxCast, while the regression benchmarks consist of FreeSolv, ESOL, and Lipophilicity. These datasets span a wide range of molecular property prediction tasks, including biophysical activity, physiological relevance, and physicochemical property estimation. Detailed statistics and task descriptions of the ten datasets are summarized in Table 2. In addition, we provide LLM-enhanced textual versions for both the ZINC15 pretraining dataset and the ten MoleculeNet finetuning datasets. These textual datasets serve as an additional semantic view during training and are publicly available on our GitHub repository.

#### Implementation Details

For graph-based contrastive learning, we employ a two-layer Attentive FP encoder to capture localized molecular patterns, such as substructure motifs and functional group information. To model global structural dependencies, we adopt a lightweight two-layer Graph Transformer encoder that is designed for efficiently capture long-range topological context across the molecular graph. During contrastive pretraining, the projection heads are applied to the outputs of both graph encoders, and the model is optimized using a contrastive loss with a temperature parameter set to 0.1. The pretraining process is conducted for 100 epochs to ensure stable convergence of the learned representations. For text-based contrastive learning, we adopt a four-layer DeBERTa encoder to model the semantic representations of molecular textual inputs. The official tokenizer provided with DeBERTa is used to tokenize

**Table 2.** Summary of benchmark datasets for molecular property prediction.

Category	Dataset	Tasks	Molecules	Task Type	Metric	Avg. nodes	Description
Biophysics	BACE	1	1513	Classification	ROC-AUC	34.1	$\beta$ -secretase inhibitory activity
	HIV	1	41127	Classification	ROC-AUC	25.5	HIV replication inhibition
Physiology	BBBP	1	2053	Classification	ROC-AUC	23.9	Blood-brain barrier permeability
	SIDER	27	1427	Classification	ROC-AUC	33.6	Drug-induced side effects
	Tox21	12	7831	Classification	ROC-AUC	18.6	Compound toxicity
	ClinTox	2	1478	Classification	ROC-AUC	26.1	Clinical toxicity
	ToxCast	617	8575	Classification	ROC-AUC	18.7	Toxicity screening(HTS)
Physical Chemistry	ESOL	1	1128	Regression	RMSE	13.3	Aqueous solubility
	FreeSolv	1	642	Regression	RMSE	8.7	Hydration free energy
	Lipophilicity	1	4200	Regression	RMSE	27.0	Compound lipophilicity(LogD)

both the original SMILES strings and their corresponding LLM-enhanced textual descriptions, ensuring consistency with the pretrained language model vocabulary. Similar to the graph-based pretraining stage, the text encoder outputs are passed through projection heads and optimized using a contrastive learning objective with the temperature parameter set to 0.1. The text-based contrastive pretraining is also conducted for 100 epochs to ensure sufficient convergence. During the fine-tuning stage, molecular fingerprint features are incorporated through a two-layer MLP to obtain fingerprint-based representations. For all downstream datasets, the model is finetuned for 50 epochs. Consistent with pretraining stages, the Adam optimizer [47] is employed during finetuning, with the initial learning rate set to  $1 \times 10^{-3}$ . All experiments were conducted on an NVIDIA RTX 4090 GPU. Regarding data splitting, we follow the random splitting protocol adopted in S-CGIB [48], using a split ratio of 0.6/0.2/0.2 for training, validation, and testing, and report the average performance over three runs with different random seeds. In addition to random splitting, we also evaluate the model under the scaffold splitting [46], which is widely regarded as a more challenging and realistic evaluation protocol for molecular property prediction. The detailed results under scaffold splitting are provided in the supplementary information.

### Baselines

To demonstrate the effectiveness of the proposed method, we compare it with a diverse set of state-of-the-art self-supervised learning baselines for molecular graph representation learning. The experimental results of these baselines are obtained under the same benchmark settings as S-CGIB [48], which we strictly follow in our experiments. These baselines can be broadly categorized into three groups.

- Predictive self-supervised methods, which learn graph representations via reconstruction or prediction-based pretext tasks without explicit contrastive objectives. The category includes ContextPred [49] and AttrMasking [49], which predict contextual or masked node attributes, as well as EdgePred [9], GraphFP [54], SimSGT [58], and MoAMA [59] that exploit edge-level fragment-level, or motif-aware masking strategies.
- Contrastive learning-based methods, which construct multiple graph views and learn representations by maximizing agreement between positive pairs. Representative approaches in this category include Infomax [50], JOAO

[51], JOAOv2 [51] and GraphCL [52], which rely on graph augmentations, as well as structure-aware contrastive methods such as GraphLoG [53], MICRO-Graph [55] and MGSSL [56].

- Advanced structural modeling methods, which employ more expressive graph architectures for molecular representation learning. This group includes GROVER [57], a graph transformer-based pretraining approach, and S-GGIB [48], which incorporates subgraph-level information constraints.

### Performance Analysis

Table 3 and Table 4 report the comparative performance of different baselines on classification and regression benchmarks, respectively. Overall, our proposed method shows robust performance across both classification and regression tasks.

On classification tasks, our method consistently improves ROC-AUC scores across challenging benchmarks such as BACE, BBBP, and ClinTox, surpassing strong pretraining approaches including GROVER and S-CGIB. In particular, the performance gains on BBBP and Tox21 demonstrate the effectiveness of our model in capturing complex molecular semantics. For regression tasks, our approach achieves the lowest RMSE on ESOL, FreeSolv, and Lipophilicity, indicating superior regression accuracy compared with existing methods. These results suggest that learned representations are more suitable for fine-grained molecular property prediction. Moreover, the relatively small standard deviations observed on several datasets indicate that our method exhibits stable and robust performance.

### Ablation Study

To assess the contribution of different molecular modalities, we perform an ablation study by varying the modality configuration while keeping the training protocol unchanged. We evaluate single-modality, bi-modality, and full-modality settings to examine the individual and joint effects of textual, graph-based, and fingerprint-based representations on downstream tasks. Table 5 reports results for three single-modality models and three bi-modality combinations, with the full model shown for reference. Performance is measured using ROC-AUC for classification tasks and RMSE for regression tasks. Overall, bi-modality consistently outperform single-modality counterparts, highlighting the importance of multimodal integration. Graph-based representations are particularly effective for regression tasks, while textual

**Table 3.** Comparative performance of different methods on classification benchmarks measured by ROC-AUC.

Methods	BACE	BBBP	ClinTox	SIDER	Tox21	ToxCast	HIV
ContextPred	78.39 $\pm$ 0.58	69.10 $\pm$ 0.29	55.63 $\pm$ 1.35	61.83 $\pm$ 0.60	73.26 $\pm$ 0.59	63.28 $\pm$ 0.68	72.04 $\pm$ 0.48
AttrMasking	75.95 $\pm$ 0.50	67.12 $\pm$ 0.45	60.11 $\pm$ 1.19	61.21 $\pm$ 0.65	73.37 $\pm$ 0.55	61.66 $\pm$ 1.20	72.71 $\pm$ 0.70
EdgePred	74.29 $\pm$ 1.37	64.73 $\pm$ 1.10	61.62 $\pm$ 1.25	60.18 $\pm$ 0.76	70.32 $\pm$ 1.62	60.04 $\pm$ 0.81	70.55 $\pm$ 1.68
Infomax	77.80 $\pm$ 0.46	68.39 $\pm$ 0.64	58.62 $\pm$ 0.83	59.02 $\pm$ 0.56	72.66 $\pm$ 0.16	62.76 $\pm$ 0.54	73.55 $\pm$ 0.47
JOAO	74.94 $\pm$ 1.35	71.63 $\pm$ 1.11	77.02 $\pm$ 1.64	63.55 $\pm$ 0.81	73.67 $\pm$ 1.06	63.30 $\pm$ 0.27	77.55 $\pm$ 1.94
JOAOv2	74.38 $\pm$ 1.71	71.98 $\pm$ 0.18	65.22 $\pm$ 0.75	59.88 $\pm$ 1.72	73.95 $\pm$ 1.88	63.12 $\pm$ 1.90	77.13 $\pm$ 1.51
GraphCL	77.80 $\pm$ 0.46	68.39 $\pm$ 0.64	61.62 $\pm$ 1.25	61.83 $\pm$ 0.60	73.26 $\pm$ 0.59	62.76 $\pm$ 0.54	73.55 $\pm$ 0.47
GraphLoG	76.60 $\pm$ 1.04	66.75 $\pm$ 0.32	53.76 $\pm$ 0.95	59.09 $\pm$ 0.53	71.64 $\pm$ 0.49	61.53 $\pm$ 0.35	73.76 $\pm$ 0.29
GraphFP	80.28 $\pm$ 3.06	72.05 $\pm$ 1.17	76.80 $\pm$ 1.83	<b>65.93 <math>\pm</math> 3.09</b>	77.35 $\pm$ 1.40	69.15 $\pm$ 1.92	75.71 $\pm$ 1.39
MICRO-Graph	63.57 $\pm$ 1.55	67.21 $\pm$ 1.85	77.56 $\pm$ 1.56	60.34 $\pm$ 0.96	71.79 $\pm$ 1.70	60.80 $\pm$ 1.15	76.73 $\pm$ 1.07
MGSSL	82.03 $\pm$ 3.79	79.52 $\pm$ 1.98	75.84 $\pm$ 1.82	57.46 $\pm$ 1.45	74.82 $\pm$ 1.60	63.86 $\pm$ 1.57	77.45 $\pm$ 2.94
GROVER	81.13 $\pm$ 0.14	87.15 $\pm$ 0.06	72.53 $\pm$ 0.14	57.53 $\pm$ 0.23	68.59 $\pm$ 0.24	64.45 $\pm$ 0.14	75.04 $\pm$ 0.13
SimSGT	79.75 $\pm$ 1.28	71.51 $\pm$ 1.75	74.11 $\pm$ 1.05	59.74 $\pm$ 1.32	76.23 $\pm$ 1.27	65.83 $\pm$ 0.79	78.13 $\pm$ 1.07
MoAMa	81.32 $\pm$ 1.06	85.89 $\pm$ 0.61	77.11 $\pm$ 1.67	62.69 $\pm$ 0.37	78.29 $\pm$ 0.55	68.01 $\pm$ 1.07	78.11 $\pm$ 0.64
S-CGIB	86.46 $\pm$ 0.81	88.75 $\pm$ 0.49	78.58 $\pm$ 2.01	64.03 $\pm$ 1.04	80.94 $\pm$ 0.17	<b>70.95 <math>\pm</math> 0.27</b>	<b>78.33 <math>\pm</math> 1.34</b>
Ours	<b>87.29 <math>\pm</math> 0.19</b>	<b>92.44 <math>\pm</math> 0.48</b>	<b>86.06 <math>\pm</math> 6.71</b>	60.49 $\pm$ 0.70	<b>81.16 <math>\pm</math> 0.71</b>	67.49 $\pm$ 0.56	77.49 $\pm$ 0.98

**Table 4.** Comparative performance of different methods on regression benchmarks measured by RMSE.

Methods	ESOL	FreeSolv	Lipophilicity
ContextPred	2.190 $\pm$ 0.026	3.195 $\pm$ 0.058	1.053 $\pm$ 0.048
AttrMasking	2.954 $\pm$ 0.087	4.023 $\pm$ 0.039	0.982 $\pm$ 0.052
EdgePred	2.368 $\pm$ 0.070	3.192 $\pm$ 0.023	1.085 $\pm$ 0.061
Infomax	2.953 $\pm$ 0.049	3.033 $\pm$ 0.026	0.970 $\pm$ 0.023
JOAO	1.978 $\pm$ 0.029	3.282 $\pm$ 0.002	1.093 $\pm$ 0.097
JOAOv2	2.144 $\pm$ 0.009	3.842 $\pm$ 0.012	1.116 $\pm$ 0.024
GraphCL	1.390 $\pm$ 0.363	3.166 $\pm$ 0.027	1.014 $\pm$ 0.018
GraphLoG	1.542 $\pm$ 0.026	2.335 $\pm$ 0.052	0.932 $\pm$ 0.052
GraphFP	2.136 $\pm$ 0.096	2.528 $\pm$ 0.016	1.371 $\pm$ 0.058
MICRO-Graph	0.842 $\pm$ 0.055	1.865 $\pm$ 0.061	0.851 $\pm$ 0.073
MGSSL	2.936 $\pm$ 0.071	2.940 $\pm$ 0.051	1.106 $\pm$ 0.077
GROVER	1.237 $\pm$ 0.403	2.712 $\pm$ 0.327	0.823 $\pm$ 0.027
SimSGT	0.932 $\pm$ 0.026	1.953 $\pm$ 0.038	0.771 $\pm$ 0.041
MoAMa	1.125 $\pm$ 0.029	2.072 $\pm$ 0.053	1.085 $\pm$ 0.024
S-CGIB	0.816 $\pm$ 0.019	1.648 $\pm$ 0.074	0.762 $\pm$ 0.042
Ours	<b>0.496 <math>\pm</math> 0.025</b>	<b>1.153 <math>\pm</math> 0.053</b>	<b>0.674 <math>\pm</math> 0.028</b>

information provides complementary chemical semantics. The full multimodal model achieves the most consistent performance across benchmarks, confirming the benefit of jointly integrating all modalities.

In addition to modality-level ablations, we further investigate the impact of different pretraining initialization strategies on downstream performance. In the original model, both text and graph encoders are initialized with pretrained parameters. We then construct three ablation settings by selectively disabling pretrained initialization, including text-only pretraining, graph-only pretraining, and a baseline trained entirely from scratch. The results are illustrated in Figure 6, which reports performance across the same six benchmark datasets using ROC-AUC for classification tasks and RMSE for regression tasks. This ablation aims to disentangle the individual and complementary contributions of text- and

graph-based pretraining, and to assess whether the observed performance gains stem from the proposed pretraining strategy rather than architectural design alone. As shown in Figure 6, full pretraining of both text and graph encoders achieves the best overall performance. Using only text or graph pretraining results in moderate degradation, while training from scratch leads to a more pronounced drop, especially on regression tasks. These results highlight the complementary contributions of text and graph pretraining. To further validate the effectiveness of contrastive learning, we additionally report single-modality ablations for text-only and graph-only models with and without pretrained initialization in the Supplementary information.

Complementary to the pretraining ablation, we investigate the effect of different aggregation strategies for multi-modal feature fusion. Our original model employs a dual cross-attention mechanism for multi-modal feature

**Table 5.** Ablation study of single- and bi-modality configurations across six molecular property prediction tasks. The best result on each dataset is bold.

Methods	BACE	BBBP	ClinTox	ESOL	FreeSolv	Lipophilicity
T	0.853	0.911	0.922	0.516	1.460	0.811
F	0.782	0.882	0.857	0.540	1.308	0.699
G	0.782	0.890	0.811	0.544	1.102	0.785
T+G	0.694	0.684	0.862	0.761	1.710	1.083
T+F	0.892	0.917	0.914	0.501	1.111	0.658
F+G	0.841	0.903	0.830	0.621	1.170	0.713
<b>T+F+G</b>	<b>0.875</b>	<b>0.929</b>	<b>0.952</b>	<b>0.478</b>	<b>1.077</b>	<b>0.634</b>

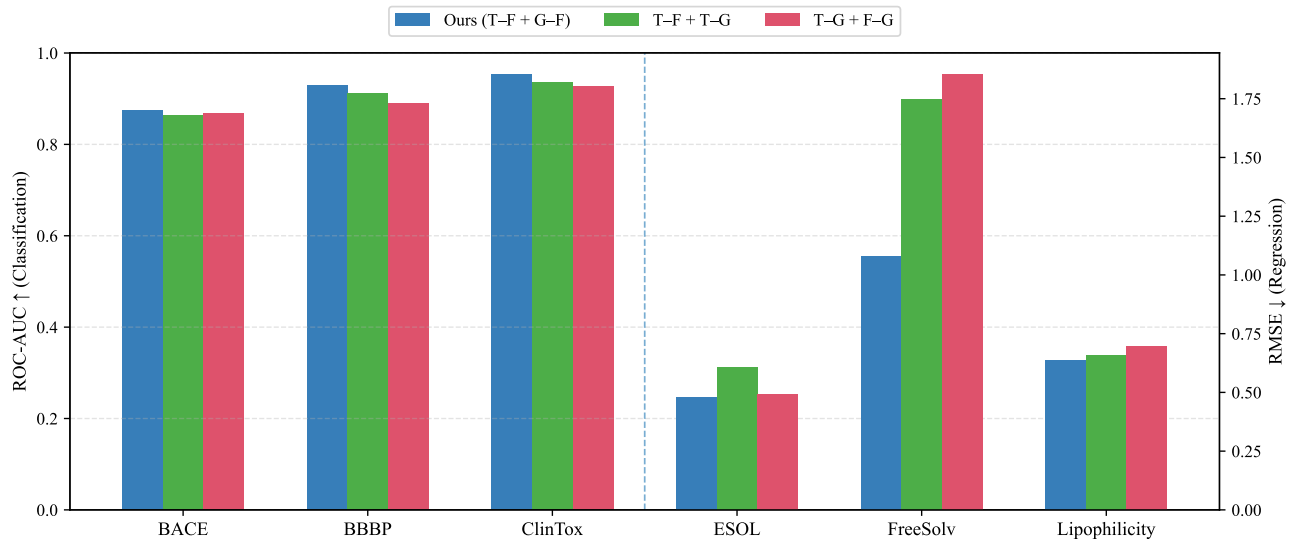


**Fig. 5.** Ablation study of dual cross-attention fusion strategies across six molecular property prediction tasks, reporting ROC-AUC for classification and RMSE for regression.

aggregation. For ablation purposes, we substitute this module with standard aggregation operations, including summation and concatenation, while keeping all other components unchanged. As shown in Figure 7, the dual cross-attention-based aggregation consistently outperforms simple summation and concatenation across both classification and regression benchmarks. This result indicates that explicitly modeling cross-modal interactions is more effective than parameter-free aggregation strategies for multi-modal feature fusion.

Finally, we conduct an ablation study on different modality pairing strategies in the dual cross-attention framework to assess their impact on multi-modal feature fusion. As shown in Figure 5, the original fingerprint-centered pairing strategy yields the most consistent performance across benchmarks, while alternative pairing schemes result in performance degradation, highlighting the importance of appropriate modality interaction design.

### Interpretability Analysis

To interpret the decision-making process of the proposed multimodal framework and quantify the contribution of each modality, we perform an interpretability analysis using SHAP (SHapley Additive exPlanations) [60]. SHAP Provides model-agnostic attributions based on Shapley values, enabling fair and additive estimation of feature contributions. In this work,

feature-level SHAP values are aggregated at the modality level to assess the relative importance of molecular fingerprints, molecular graphs, and texts in the final prediction.

The modality-level SHAP contributions across multiple benchmark datasets are shown in Figure 8. The result exhibit clear task-dependent differences. For datasets such as BACE, BBBP, ClinTox, SIDER, ESOL, and FreeSolv, fingerprint representations dominate the predictions, contributing the majority of the overall importance, while graph- and text-based modalities play a minor role. This suggests that, for these tasks, compact substructure patterns encoded in fingerprints are sufficient to capture the key determinants of molecular properties. In contrast, more complex datasets such as Tox21 and HIV display a more balanced contribution across modalities, including that accurate prediction requires the joint use of structural, topological, and semantic information. The Toxcast dataset shows a similar trend, with fingerprints and graph representations jointly contributing most of the predictive signal, and textual information providing complementary support. For Lipophilicity, the text modality exhibits a relatively higher contribution, highlighting the importance of physicochemical information beyond purely structural descriptors for this task.

Overall, this analysis demonstrates that the proposed framework adaptively leverages different modalities depending

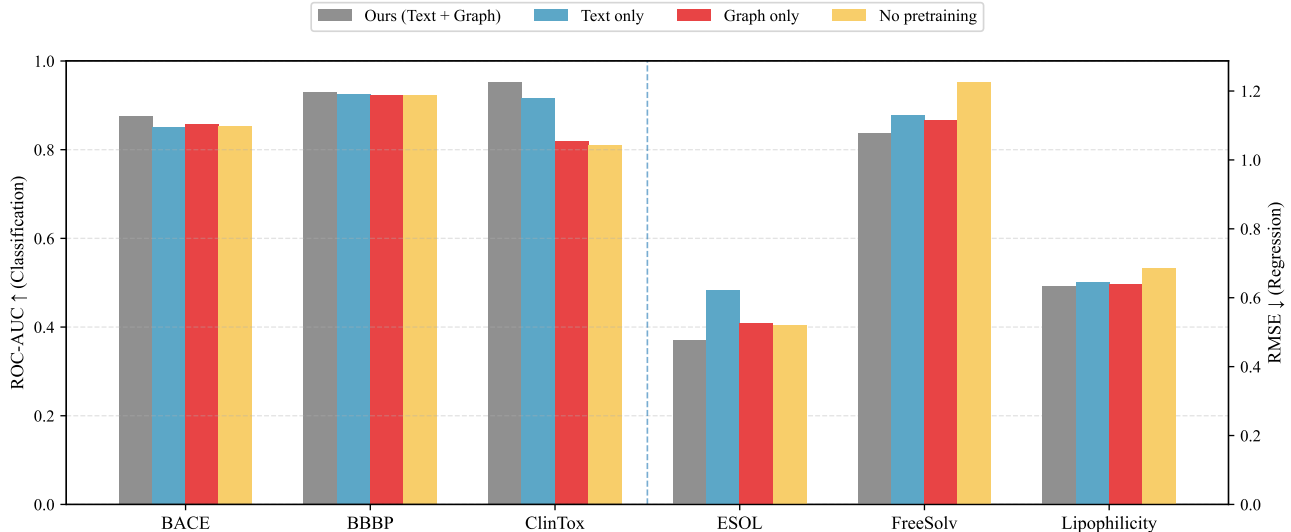


**Fig. 6.** Ablation study of different pretraining initialization strategies across six molecular property prediction tasks, reporting ROC-AUC for classification and RMSE for regression.

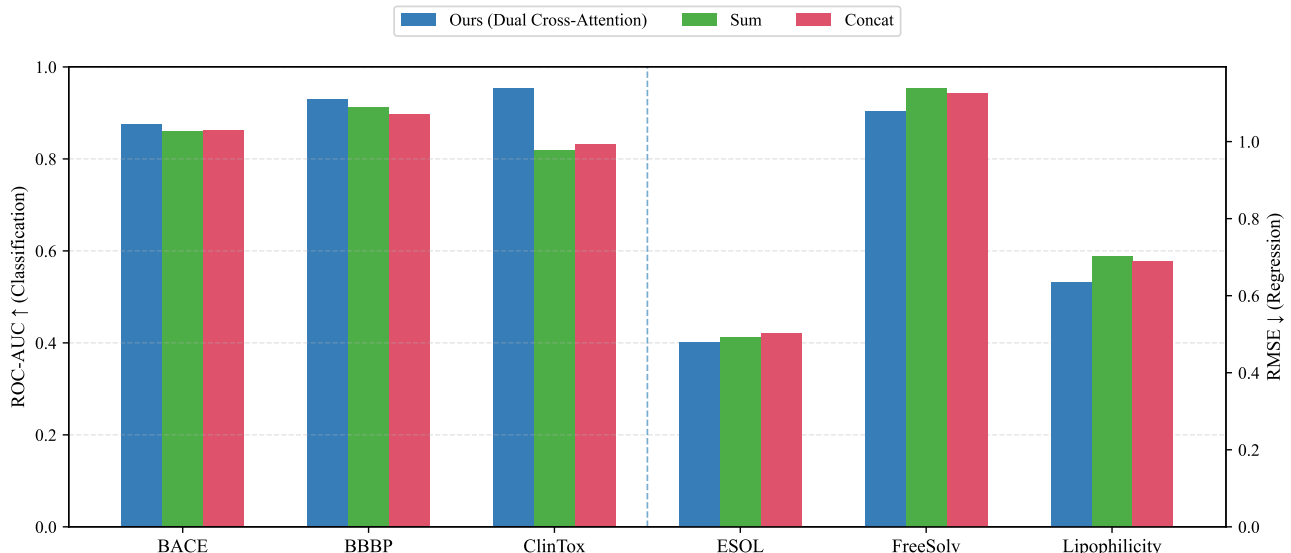


**Fig. 7.** Ablation study of different feature fusion strategies across six molecular property prediction tasks, reporting ROC-AUC for classification and RMSE for regression.

on the prediction task, rather than relying on a single information source. The SHAP-based results provide quantitative evidence for the effectiveness of multi-modal integration, particularly for challenging molecular property prediction problems where heterogeneous information sources are essential.

To gain an intuitive understanding of the learned molecular representations, we employ t-SNE [61], a widely used nonlinear dimensionality reduction technique for visualizing high-dimensional data in a low-dimensional space. t-SNE maps samples into a two-dimensional embedding by preserving local neighborhood similarities, enabling the inspection of structural patterns and class separability in the learned feature space.

Figure 9 presents the t-SNE visualizations of the model representations on the test sets of several benchmark datasets, obtained under the random splitting protocol with a ratio

of 0.6/0.2/0.2. For classification tasks (BACE, BBBP, and ClinTox), different colors denote different class labels, while for regression tasks (ESOL and Lipophilicity), the color intensity reflects the magnitude of the target property. In addition, we also provide t-SNE visualization of models trained under the scaffold splitting protocol in the supplementary material.

Overall, the visualizations indicate that the learned representations exhibit meaningful organization in the embedding space. In several datasets, samples with similar labels or property values tend to form coherent clusters or follow smooth structural trends, suggesting that the model captures task-relevant molecular characteristics. Those observations provide qualitative evidence that the proposed representation learning framework produces informative and discriminative embeddings.

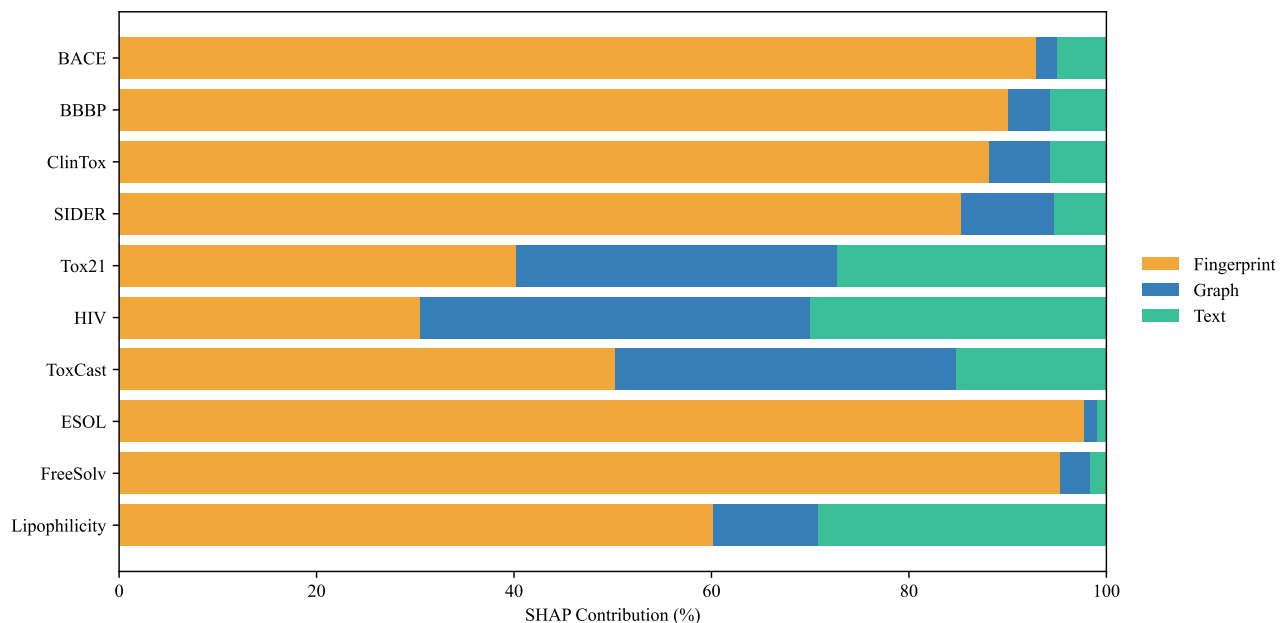


**Fig. 8.** Dataset-dependent modality contribution revealed by SHAP analysis.

## Conclusion

In this work, we proposed LGM-CL, a local-global multimodal contrastive learning framework for molecular property prediction. By jointly modeling local functional group and global molecular topology from molecular graphs, and aligning them with chemistry-aware textual representations derived from SMILES and augmented texts, the proposed method learns transferable and chemically meaningful molecular embeddings. During fine-tuning, molecular fingerprints are further integrated through dual cross-attention module to enhance downstream prediction. Extensive experiments on MoleculeNet benchmarks demonstrate that LGM-CL achieves consistent and competitive performance across both classification and regression tasks. Ablation and interpretability analyses further validate the complementary contributions of different modalities. These results highlight the effectiveness of unified local-global and multimodal representation learning for molecular property prediction.

## Key points

- We propose a local-global multimodal contrastive learning framework that jointly models fine-grained local chemical patterns and global molecular structural dependencies.
- A chemistry-aware text augmentation strategy is introduced to align SMILES with enriched physicochemical semantics through contrastive learning in a self-supervised manner.
- A dual cross-attention fusion mechanism effectively integrates graph, text and fingerprint representations for unified molecular representation learning.
- Extensive experiments on MoleculeNet benchmarks demonstrate consistent and robust performance gains across both classification and regression tasks, supported by comprehensive ablation and interpretability analysis.

## Competing interests

The authors declare no competing financial interest.

## Data availability

The datasets used in the experiments, along with their corresponding text-augmented versions, are publicly available at <https://github.com/lhb0189/LGM-CL>.

## Acknowledgments

This work is supported by National Natural Science Foundation of China (Grant: 11101071). Supported by Center for HPC, University of Electronic Science and technology.

## References

1. Jorissen, Robert N and Gilson, Michael K. Virtual screening of molecular databases using a support vector machine. *Journal of chemical information and modeling*, 45(3):549–561, 2005.
2. Mahé, Pierre and Ralaivola, Liva and Stoven, Véronique and Vert, Jean-Philippe. The pharmacophore kernel for virtual screening with support vector machines. *Journal of chemical information and modeling*, 46(5):2003–2014, 2006.
3. Svetnik, Vladimir and Liaw, Andy and Tong, Christopher and Culberson, J Christopher and Sheridan, Robert P and Feuston, Bradley P. Random forest: a classification and regression tool for compound classification and QSAR modeling. *Journal of chemical information and computer sciences*, 43(61):1947–1958, 2003.
4. Cortes, Corinna and Vapnik, Vladimir. Support-vector networks. *Machine learning*, 20(3):273–297, 1995.
5. Breiman, Leo. Random forests. *Machine learning*, 45(1):5–32, 2001.

6. Duvenaud, David K and Maclaurin, Dougal and Iparraguirre, Jorge and Bombarell, Rafael and Hirzel, Timothy and Aspuru-Guzik, Alán and Adams, Ryan P. Convolutional networks on graphs for learning molecular fingerprints. *Advances in neural information processing systems*, 28, 2015.

7. Gilmer, Justin and Schoenholz, Samuel S and Riley, Patrick F and Vinyals, Oriol and Dahl, George E. Neural message passing for quantum chemistry. *International conference on machine learning*, 1263–1272, 2017.

8. Kipf, TN. Semi-supervised classification with graph convolutional networks. *arXiv preprint arXiv:1609.02907*, 2016.

9. Hamilton, Will and Ying, Zhitao and Leskovec, Jure. Inductive representation learning on large graphs. *Advances in neural information processing systems*, 30, 2017.

10. Petar Veličković and Guillem Cucurull and Arantxa Casanova and Adriana Romero and Pietro Lio and Yoshua Bengio. Graph attention networks. *arXiv preprint arXiv:1710.10903*, 2017.

11. Xu, Keyulu and Hu, Weihua and Leskovec, Jure and Jegelka, Stefanie. How powerful are graph neural networks?. *arXiv preprint arXiv:1810.00826*, 2018.

12. Chen, Zhe and Tan, Hao and Wang, Tao and Shen, Tianrun and Lu, Tong and Peng, Qiuying and Cheng, Cheng and Qi, Yue. Graph propagation transformer for graph representation learning. *Proceedings of the Thirty-Second International Joint Conference on Artificial Intelligence*, 3559–3567, 2023.

13. Luo, Shengjie and Chen, Tianlang and Xu, Yixian and Zheng, Shuxin and Liu, Tie-Yan and Wang, Liwei and He, Di. One transformer can understand both 2d & 3d molecular data. *arXiv preprint arXiv:2210.01765*, 2022.

14. Ying, Chengxuan and Cai, Tianle and Luo, Shengjie and Zheng, Shuxin and Ke, Guolin and He, Di and Shen, Yanming and Liu, Tie-Yan. Do transformers really perform badly for graph representation?. *Advances in neural information processing systems*, 34:28877–28888, 2021

15. Vaswani, Ashish and Shazeer, Noam and Parmar, Niki and Uszkoreit, Jakob and Jones, Llion and Gomez, Aidan N and Kaiser, Łukasz and Polosukhin, Illia. Attention is all you need. *Advances in neural information processing systems*, 30, 2017.

16. Morgan, Harry L. The generation of a unique machine description for chemical structures-a technique developed at chemical abstracts service. *Journal of chemical documentation*, 5(2):107–113, 1965.

17. Gasteiger, Johannes and Grok, Janek and Günemann, Stephan. Directional message passing for molecular graphs. *arXiv preprint arXiv:2003.03123*, 2020.

18. Weininger, David. SMILES, a chemical language and information system. 1. Introduction to methodology and encoding rules. *Journal of chemical information and computer sciences*, 28(1):31–36, 1988.

19. Chithrananda, Seyone and Grand, Gabriel and Ramsundar, Bharath. ChemBERTa: large-scale self-supervised pretraining for molecular property prediction. *arXiv preprint arXiv:2010.09885*, 2020.

20. Zhang, Tianyu and Ren, Yuxiang and Hou, Chengbin and Lv, Hairong and Zhang, Xuegong. Molecular graph representation learning integrating large language models with domain-specific small models. *2024 IEEE International Conference on Bioinformatics and Biomedicine (BIBM)*, 2928–2935, 2024.

21. Guo, Haoqiang and Zhao, Sendong and Wang, Haochun and Du, Yanrui and Qin, Bing. MolTailor: tailoring chemical molecular representation to specific tasks via text prompts. *Proceedings of the AAAI Conference on Artificial Intelligence*, 38(16):18144–18152, 2024.

22. Zheng, Yizhen and Koh, Huan Yee and Ju, Jiaxin and Nguyen, Anh TN and May, Lauren T and Webb, Geoffrey I and Pan, Shirui. Large language models for scientific synthesis, inference and explanation. *arXiv preprint arXiv:2310.07984*, 2023.

23. Xu, Ziwei and Jain, Sanjay and Kankanhalli, Mohan. Hallucination is inevitable: An innate limitation of large language models. *arXiv preprint arXiv:2401.11817*, 2024.

24. Zhang, Haohui and Wu, Junlong and Liu, Shichao and Han, Shen. A pre-trained multi-representation fusion network for molecular property prediction. *Information Fusion*, 103:102092, 2024.

25. Liu, Pengfei and Ren, Yiming and Tao, Jun and Ren, Zhixiang. Git-mol: A multi-modal large language model for molecular science with graph, image, and text. *Computers in biology and medicine*, 171:108073, 2024.

26. Sun, Mengying and Xing, Jing and Wang, Huijun and Chen, Bin and Zhou, Jiayu. MoCL: data-driven molecular fingerprint via knowledge-aware contrastive learning from molecular graph. *Proceedings of the 27th ACM SIGKDD conference on knowledge discovery & data mining*, 3585–3594, 2021.

27. Chen, Ting and Kornblith, Simon and Norouzi, Mohammad and Hinton, Geoffrey. A simple framework for contrastive learning of visual representations. *International conference on machine learning*, 1597–1607, 2020.

28. Radford, Alec and Kim, Jong Wook and Hallacy, Chris and Ramesh, Aditya and Goh, Gabriel and Agarwal, Sandhini and Sastray, Girish and Askell, Amanda and Mishkin, Pamela and Clark, Jack and others. Learning transferable visual models from natural language supervision. *International conference on machine learning*, 8748–8763, 2021.

29. Zhaoping Xiong and Dingyan Wang and Xiaohong Liu and Feisheng Zhong and Xiaozhe Wan and Xutong Li and Zhaojun Li and Xiaomin Luo and Kaixian Chen and Hualiang Jiang and others. Pushing the boundaries of molecular representation for drug discovery with the graph attention mechanism. *Journal of Medicinal Chemistry*, 63(16):8749–8760, 2019.

30. Xiuyu Jiang and Liqin Tan and Qingsong Zou. DGCL: dual-graph neural networks contrastive learning for molecular property prediction. *Briefings in Bioinformatics*, 25(6):bbae474, 2024.

31. Albert Qiaochu Jiang and Alexandre Sablayrolles and Arthur Mensch and Chris Bamford and Devendra Singh Chaplot and Diego de Las Casas and Florian Bressand and Gianna Lengyel and Guillaume Lample and Lucile Saulnier and L'elio Renard Lavaud and Marie-Anne Lachaux and Pierre Stock and Teven Le Scao and Thibaut Lavril and Thomas Wang and Timothée Lacroix and William El Sayed. Mistral 7B. *arXiv preprint arXiv:2307.04657*, 2023.

32. He, Pengcheng and Liu, Xiaodong and Gao, Jianfeng and Chen, Weizhu. Deberta: Decoding-enhanced bert with disentangled attention. *arXiv preprint arXiv:2006.03654*, 2020.

33. Maziarka, Łukasz and Danel, Tomasz and Mucha, Sławomir and Rataj, Krzysztof and Tabor, Jacek and Jastrzębski, Stanisław. Molecule attention transformer. *arXiv preprint*

*arXiv:2002.08264*, 2020.

34. Maziarka, Łukasz and Majchrowski, Dawid and Danel, Tomasz and Gaiński, Piotr and Tabor, Jacek and Podolak, Igor and Morkisz, Paweł and Jastrzębski, Stanisław. Relative molecule self-attention transformer. *Journal of Cheminformatics*, 16(1):3, 2024.
35. Yun, Seongjun and Jeong, Minbyul and Kim, Rae hyun and Kang, Jaewoo and Kim, Hyunwoo J. Graph transformer networks. *Advances in neural information processing systems*, 32, 2019.
36. Liu, XiaYu and Fan, Chao and Liu, Yang and Li, Hou-biao. Multilevel Fusion Graph Neural Network for Molecule Property Prediction. *Journal of Chemical Information and Modeling*, 65(17):9034–9048, 2025.
37. Chung, Junyoung and Gulcehre, Caglar and Cho, KyungHyun and Bengio, Yoshua. Empirical evaluation of gated recurrent neural networks on sequence modeling. *arXiv preprint arXiv:1412.3555*, 2014.
38. Durant, Joseph L and Leland, Burton A and Henry, Douglas R and Nourse, James G. Reoptimization of MDL keys for use in drug discovery. *Journal of chemical information and computer sciences*, 42(6):1273–1280, 2002.
39. Bolton, Evan E and Wang, Yanli and Thiessen, Paul A and Bryant, Stephen H. PubChem: integrated platform of small molecules and biological activities. *Annual reports in computational chemistry*, 4:217–241, 2008.
40. Stiefl, Nikolaus and Watson, Ian A and Baumann, Knut and Zaliani, Andrea. ErG: 2D pharmacophore descriptions for scaffold hopping. *Journal of chemical information and modeling*, 46(1):208–220, 2006.
41. Wu, Zhenqin and Ramsundar, Bharath and Feinberg, Evan N and Gomes, Joseph and Geniesse, Caleb and Pappu, Aneesh S and Leswing, Karl and Pande, Vijay. MoleculeNet: a benchmark for molecular machine learning. *Chemical science*, 9(2):513–530, 2018.
42. Jin, Chang and Guo, Siyuan and Zhou, Shuigeng and Guan, Jihong. Effective and Explainable Molecular Property Prediction by Chain-of-Thought Enabled Large Language Models and Multi-Modal Molecular Information Fusion. *Journal of Chemical Information and Modeling*, 65(11):5438–5455, 2025.
43. Li, Na and Qiao, Jianbo and Gao, Fei and Wang, Yanling and Shi, Hua and Zhang, Zilong and Cui, Feifei and Zhang, Lichao and Wei, Leyi. GICL: A Cross-Modal Drug Property Prediction Framework Based on Knowledge Enhancement of Large Language Models. *Journal of Chemical Information and Modeling*, 2025.
44. Zhang, Ru and Lin, Yanmei and Wu, Yijia and Deng, Lei and Zhang, Hao and Liao, Mingzhi and Peng, Yuzhong. MvMRL: a multi-view molecular representation learning method for molecular property prediction. *Briefings in Bioinformatics*, 25(4):bbae298, 2024.
45. Sterling, Teague and Irwin, John J. ZINC 15-ligand discovery for everyone. *Journal of chemical information and modeling*, 55(11):2324–2337, 2015.
46. Bemis, Guy W and Murcko, Mark A. The properties of known drugs. 1. Molecular frameworks. *Journal of medicinal chemistry*, 39(15):2887–2893, 1996.
47. Kingma, Diederik P. Adam: A method for stochastic optimization. *arXiv preprint arXiv:1412.6980*, 2014.
48. Lee, O-Joun and others. Pre-Training Graph Neural Networks on Molecules by Using Subgraph-Conditioned Graph Information Bottleneck. *Proceedings of the AAAI Conference on Artificial Intelligence*, 39(16):17204–17213.
49. Hu, Weihua and Liu, Bowen and Gomes, Joseph and Zitnik, Marinka and Liang, Percy and Pande, Vijay and Leskovec, Jure. Strategies for pre-training graph neural networks. *arXiv preprint arXiv:1905.12265*, 2019.
50. Veličković, Petar and Fedus, William and Hamilton, William L and Liò, Pietro and Bengio, Yoshua and Hjelm, R Devon. Deep graph infomax. *arXiv preprint arXiv:1809.10341*, 2018.
51. You, Yuning and Chen, Tianlong and Shen, Yang and Wang, Zhangyang. Graph contrastive learning automated. *International conference on machine learning*, 12121–12132, 2021.
52. You, Yuning and Chen, Tianlong and Sui, Yongduo and Chen, Ting and Wang, Zhangyang and Shen, Yang. Graph contrastive learning with augmentations. *Advances in neural information processing systems*, 33:5812–5823, 2020.
53. Xu, Minghao and Wang, Hang and Ni, Bingbing and Guo, Hongyu and Tang, Jian. Self-supervised graph-level representation learning with local and global structure. *International conference on machine learning*, 11548–11558, 2021.
54. Subramonian, Arjun. Motif-driven contrastive learning of graph representations. *Proceedings of the AAAI conference on artificial intelligence*, 35(18):15980–15981, 2021.
55. Zhang, Zaixi and Liu, Qi and Wang, Hao and Lu, Chengqiang and Lee, Chee-Kong. Motif-based graph self-supervised learning for molecular property prediction. *Advances in Neural Information Processing Systems*, 34:15870–15882, 2021.
56. Luong, Kha-Dinh and Singh, Ambuj K. Fragment-based pretraining and finetuning on molecular graphs. *Advances in Neural Information Processing Systems*, 36:17584–17601, 2023.
57. Rong, Yu and Bian, Yatao and Xu, Tingyang and Xie, Weiyang and Wei, Ying and Huang, Wenbing and Huang, Junzhou. Self-supervised graph transformer on large-scale molecular data. *Advances in neural information processing systems*, 33:12559–12571, 2020.
58. Liu, Zhiyuan and Shi, Yaorui and Zhang, An and Zhang, Enzhi and Kawaguchi, Kenji and Wang, Xiang and Chua, Tat-Seng. Rethinking tokenizer and decoder in masked graph modeling for molecules. *Advances in Neural Information Processing Systems*, 36:25854–25875, 2023.
59. Inae, Eric and Liu, Gang and Jiang, Meng. Motif-aware attribute masking for molecular graph pre-training. *arXiv preprint arXiv:2309.04589*, 2023.
60. Lundberg, Scott M and Lee, Su-In. A unified approach to interpreting model predictions. *Advances in neural information processing systems*, 30, 2017.
61. Maaten, Laurens van der and Hinton, Geoffrey. Visualizing data using t-SNE. *Journal of Machine Learning Research*, 9:2579–2605, 2008.

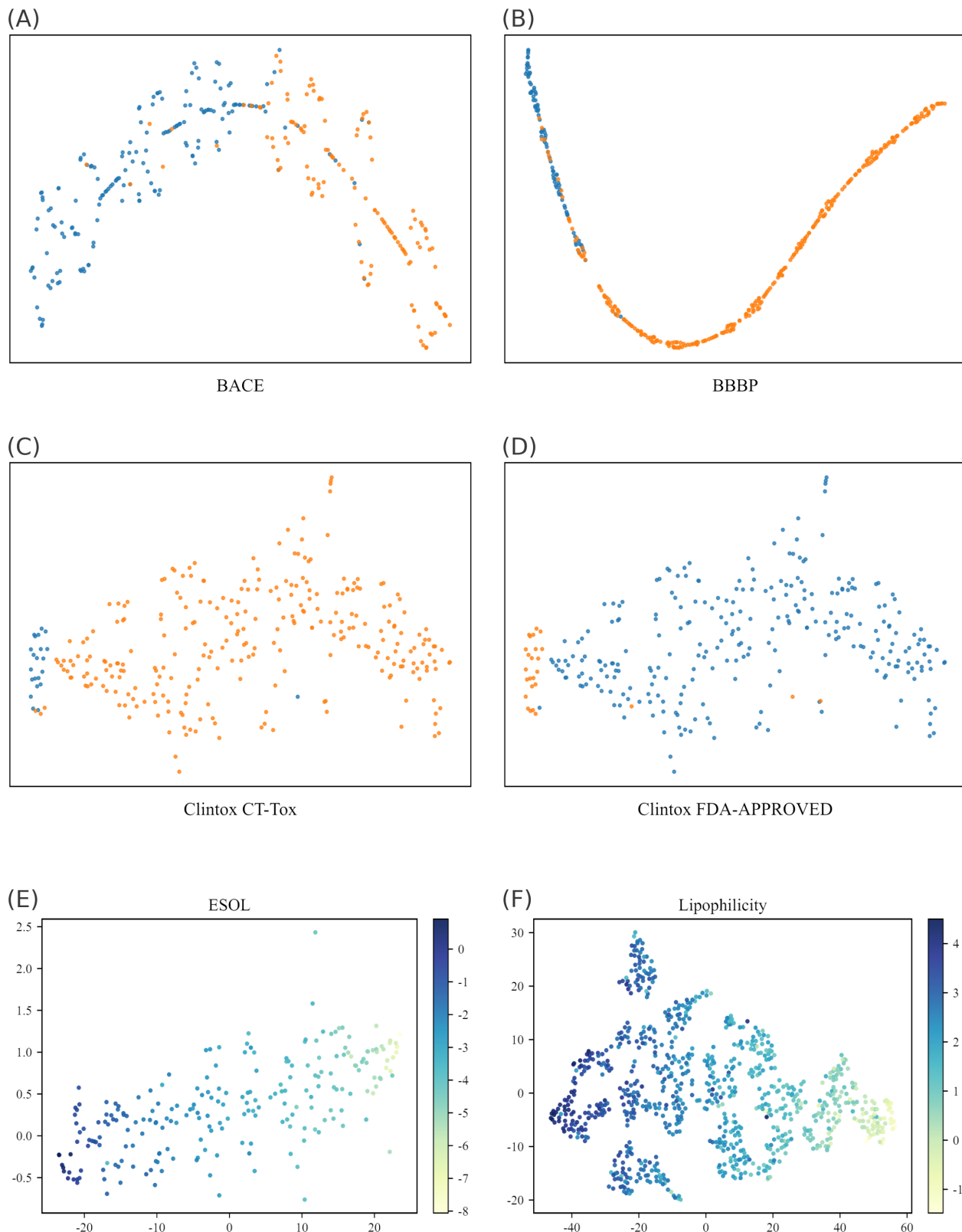


**Fig. 9.** t-SNE visualizations of learned molecular representations on the test sets. (A) BACE. (B) BBBP. (C) ClinTox(CT-Tox). (D) ClinTox(FDA-APPROVED). (E) ESOL. (F) Lipophilicity. For classification tasks, different colors indicate different class labels, while for regression tasks, the color gradient reflects the corresponding target property values. The visualizations illustrate the organization of molecular embeddings learned by the model in a two-dimensional space.